IEEE Access
Multidisciplinary ⋮ Rapid Review ⋮ Open Access Journal

Received 1 September 2025, accepted 14 September 2025,
date of publication 18 September 2025, date of current version 24 September 2025.

Digital Object Identifier 10.1109/ACCESS.2025.3611486

RESEARCH ARTICLE

Rethinking Persistent Scheduling in 5G New Radio Vehicle-to-Everything Sidelink Communications

ALEXEY ROLICH[1], (Member, IEEE), MERT YILDIZ[1], (Graduate Student Member, IEEE), ION TURCANU[2], (Senior Member, IEEE), ALEXEY VINEL[3], (Senior Member, IEEE), AND ANDREA BAIOCCHI[1], (Member, IEEE)

[1]Department of Information Engineering, Electronics and Telecommunications (DIET), University of Rome Sapienza, 00185 Rome, Italy
[2]Luxembourg Institute of Science and Technology (LIST), 4362 Esch-sur-Alzette, Luxembourg
[3]Karlsruhe Institute of Technology (KIT), 76131 Karlsruhe, Germany

Corresponding author: Alexey Rolich (alexey.rolich@uniroma1.it)

This work was supported in part by Sapienza University of Rome in the Scope of "Progetti per Avvio alla Ricerca-Tipo 2," in 2024, through the Project "Enhancing Resource Allocation Mechanisms in 5G NR-V2X Sidelink Communications: Optimization and Performance Evaluation," under Grant AR2241906D14C736, and through the Project "Modeling and Optimization of Sidelink Communications in C-V2X 5G NR," under Grant RP123188F68315A5; in part by the Ministry of University and Research of Italy through the PRIN Program under Project 20223Y85JN and through the Project "LOREN—Low-Delay Congestion Control for Real-Time Applications Over the Internet" under Grant CUP: B53D23002200006; and in part by Luxembourg National Research Fund (FNR) under the Project CANDI under Grant INTER/ANR/22/17192457.

ABSTRACT 5G New Radio (NR) Vehicle-to-Everything (V2X) Mode 2 relies on Semi-Persistent Scheduling (SPS) to manage sidelink resources, with persistence playing a key role in affecting communication integrity and Age of Information (AoI) for connected and autonomous vehicles. However, its impact remains underexplored, and whether to include SPS as is in future standards remains an open issue, calling for a deeper understanding of its effects. In this paper, we introduce a simpler method for implementing the persistence concept in 5G NR-V2X Mode 2, providing a broader range of persistence degrees than standard SPS. Through ns-3 simulations, we show that higher persistence improves communication stability, but it degrades the AoI by slowing sub-channel switching. Conversely, weaker persistence strikes a better balance between collision occurrence rate and collision duration, minimizing AoI. Crucially, our results reveal that Dynamic Scheduling (DS) can outperform SPS even for strictly periodic traffic flows, challenging the longstanding assumption that SPS is optimal in such scenarios. In fact, it turns out that persistent collisions boost message delivery burstiness, creating large gaps in the flow of delivered update messages. Our findings offer clearer guidance on designing simpler, more effective sidelink multiple access strategies to improve communication timeliness.

INDEX TERMS 5G, V2X, semi-persistent scheduling, sidelink communications, age of information, autonomous resource selection, dynamic scheduling, persistence, vehicular networks.

I. INTRODUCTION

Cooperative awareness and collective perception are key enablers for Intelligent Transportation Systems (ITS) applications such as connected and autonomous driving, virtual train coupling [1], and cooperative industrial vehicles [2]. 5G New Radio (NR) Vehicle-to-Everything (V2X) [3] supports these applications through sidelink Mode 2, where users autonomously select and reserve resources for direct Vehicle-to-Vehicle (V2V) communication without

The associate editor coordinating the review of this manuscript and approving it for publication was Nurul I. Sarkar.

relying on base stations. Two access protocols are defined: Dynamic Scheduling (DS) and Semi-Persistent Scheduling (SPS) [4], [5], [6].

SPS is tailored to periodic traffic, e.g., Cooperative Awareness Message (CAM) and Basic Safety Message (BSM). Vehicles sense the channel to identify free time-frequency slots and reserve them for multiple consecutive transmissions (*persistent scheduling*) at a fixed Resource Reservation Interval (RRI). While persistence reduces signaling and interference, collisions still occur when vehicles select the same resource. Such collisions may persist for many transmissions, effectively modeling the channel as Gilbert–Elliot [7], [8], but this effect has not been validated under realistic conditions with hidden nodes and Sub-Channels (SCs) reuse.

Current standards [4], [5], [6], [9], [10], [11] define limited persistence settings through parameters such as Reselection Counter (RC) and probability of persistence (P), without clarifying their rationale or exploring broader configurations. Moreover, existing evaluations [12], [13], [14], [15], [16], [17], [18], [19], [20], [21], [22], [23], [24], [25], [26], [27], [28], [29], [30], [31], [32], [33], [34], [35], [36] largely emphasize reliability metrics such as Packet Reception Ratio (PRR), Packet Inter-Reception Time (PIR) [10], Collision Loss Ratio (CLR) and Propagation Loss Ratio (PLR), whereas the Age of Information (AoI) [37], [38], [39], [40], [41], which directly measures the timeliness of updates, is more relevant for safety-critical cooperative maneuvers. Despite its relevance, the impact of persistence on AoI has been scarcely investigated.

This paper addresses these gaps and makes three main contributions:

1) We introduce a new way for implementing persistence in 5G NR-V2X communications, called Geometric Semi-Persistent Scheduling (G-SPS). This approach offers a broader range of persistence configurations compared to the existing SPS. It is easier to implement, requiring only a single parameter, unlike SPS, which needs multiple parameters. It also exhibits better tail properties, e.g., smaller probability of losing several messages in a row.
2) We show that optimal AoI performance, both in terms of mean value and quantiles, can be achieved with persistence settings that are only achievable with the proposed G-SPS and are outside the current standard SPS scope.
3) Our results indicate that AoI performance achieved with DS is comparable to or even better than those achieved by using persistent scheduling, suggesting that DS can be a more effective option from an AoI perspective. The significance of this insight stems from the fact that we consistently consider scenarios with *periodic* message traffic flows.

The rest of the paper is structured as follows. Section II reviews related work on persistence in 5G NR-V2X. Section III presents the proposed G-SPS and its advantages over standardized SPS. Section IV introduces the performance metrics, while Section V details the simulation environment. Section VI and Section VII report integrity and timeliness results, respectively. Finally, Section VIII summarizes the findings and outlines future research directions. Table 1 lists the acronyms used throughout the paper.

TABLE 1. List of acronyms.

Acronym	Meaning
AoI	Age of Information
BLER	Block-Error Rate
CAM	Cooperative Awareness Message
CLR	Collision Loss Ratio
C-V2X	Cellular V2X
DS	Dynamic Scheduling
G-SPS	Geometric Semi-Persistent Scheduling
MAC	Medium Access Control
MCS	Modulation and Coding Scheme
NR	New Radio
P	Probability of Persistence
PDF	Probability Distribution Function
PIR	Packet Inter-Reception Time
PLR	Propagation Loss Ratio
PRR	Packet Reception Ratio
RB	Resource Block
RC	Reselection Counter
RE	Resource Element
RRI	Resource Reservation Interval
RSSI	Received Signal Strength Indicator
RSRP	Reference Signal Receive Power
SC	Sub-Channel
SCS	Sub-Carrier Spacing
SNR	Signal-to-Noise Ratio
SNIR	Signal-to-Noise-plus-Interference Ratio
SPS	Semi-Persistent Scheduling
TB	Transport Block
V2X	Vehicle-to-Everything
WBS	Wireless Blind Spot

II. BACKGROUND AND RELATED WORK

This section examines related research efforts aimed at enhancing resource allocation efficiency in 5G NR-V2X communications. Specifically, it focuses on persistence management strategies, including the regulation of parameters such as RC and P, to optimize performance of resource allocation algorithms.

The study by Bazzi et al. [42] examines the issue of Wireless Blind Spots (WBSs) in autonomous Cellular V2X (C-V2X) communication, where vehicles may experience prolonged packet loss due to factors such as hidden nodes, half-duplex transceivers, and random resource selection. The authors characterize the probability of WBS and propose an enhanced resource allocation algorithm that limits incorrect reservations, indirectly affecting SPS with different values of P.

The influence of P on C-V2X performance is further explored by Bazzi et al. [43], who identify a trade-off between reliability and latency in 3GPP Mode 4. While higher persistence values stabilize resource allocations and improve PRR, they also increase update delays in congested environments. The study highlights the need for adaptable persistence settings to balance these conflicting metrics.

In the context of 5G NR-V2X, Yoon et al. [44] address the shortcomings of standard SPS for aperiodic traffic. They propose Reservation for Aperiodic Packets (RAP) scheme, a stochastic reservation method that enhances PRR and extends the Tx-Rx range by up to 75 m, particularly at lower P. This underscores the potential for refined algorithms to mitigate uncertainties in dynamic traffic scenarios.

Several works, such as [21], [23] and [45], compare the effectiveness of SPS and alternative schemes under various traffic types and persistence settings. While in this works SPS performs well for periodic traffic, adaptive scheduling strategies prove beneficial in mixed traffic scenarios. These studies, however, often fail to explore the full impact of persistence parameters on key metrics such as AoI.

A notable effort by Cao et al. [46] investigates the relationship between RRI, P, and PIR, showing that optimal RRI settings significantly enhance performance across different densities. Their work complements research into persistence-driven enhancements but leaves room for further exploration of dynamic configurations.

Building on the importance of dynamic resource allocation, Lusvarghi et al. [20] introduce a machine learning-based approach for aperiodic CAMs in V2V communication. Their method predicts message generation patterns and adjusts RC dynamically, achieving efficient persistence management within the standard P range. This innovation improves collision avoidance and enhances LTE-V2X Mode 4 performance by aligning resource reservations with short-term traffic patterns.

Security considerations are addressed in [47], where a persistence-aware SPS framework integrating attack detection mechanisms to adjust RC dynamically is proposed. This approach demonstrates the utility of persistence management for both congestion control and intrusion resilience. Similarly, Rolich et al. [48] leverage persistence to optimize AoI in decentralized congestion control algorithms, highlighting its role in improving system performance under diverse conditions.

The studies presented in [7], [8] were among the first to analyze persistence as a critical parameter in SPS, identifying optimal levels to minimize AoI and validating findings through realistic simulations in highway scenarios. Rolich et al. [49] study the effect of persistence on temporal and spatial reuse in sidelink communication, showing that while it improves spatial reuse, it can degrade temporal freshness by increasing AoI. However, these works focused on simpler setups where all nodes were within the same awareness range, without addressing the more complex hidden node scenarios involving spatial reuse of radio resources and dynamic traffic conditions.

Our paper makes a significant contribution to the literature by systematically analyzing persistence as a unified parameter combining the effects of RC and P for the first time. Unlike previous studies that treated RC and P independently, we investigate deeply their joint influence as a single cohesive phenomenon. This novel perspective allows us to assess the comprehensive impact of persistence on reliability, timeliness, and, critically, AoI in 5G NR-V2X networks under hidden node scenarios with periodic update message flows. By addressing this previously unexplored aspect, our work bridges a crucial gap in understanding how persistence governs sidelink performance in dynamic and challenging environments. Furthermore, we propose an innovative persistence management framework that extends existing algorithms, providing optimized resource allocation strategies to meet the stringent requirements of 5G NR-V2X communications.

III. DEFINING AND IMPLEMENTING PERSISTENCE

This section provides an overview of the standardized multiple access algorithms SPS (Section III-A) and DS (Section III-B). Then, it proposes G-SPS, a variant of SPS characterized by a new way to implement persistence (Section III-C). Finally, a systematic classification of persistence, that justifies the new proposed G-SPS, is presented in Section III-D. For a comprehensive description of SPS mechanisms, we refer the reader to [3], [8].

A. SEMI-PERSISTENT SCHEDULING (SPS)

The key idea of SPS is to keep a selected SC for a number of consecutive time periods, referred to as RRIs. This approach matches periodic traffic patterns by avoiding a randomized selection process that is prone to collisions when it can be anticipated that new messages will be generated regularly, with a given period, corresponding to the chosen RRI value.

The standard SPS mechanism relies on two parameters to ensure resource persistence:

- RC, initialized to a non-negative integer value and decremented in each subsequently used SC.
- The persistence probability P, set to a value in the range [0; 0.8].

When a new SC is selected at time t_0, the node initializes the RC with a value r. At each subsequent transmission, occurring at times $t_0 + k \cdot \text{RRI}$, the counter is decremented, and the node records its value as $r - k$, for $k = 0, 1, \ldots, r$. When the SC is used for the $(r+1)$-th time, the node decides to persist using the same SC with probability P. If the node persists using the same SC, a new initial value for the RC is randomly drawn and the countdown is restarted.

The RC value depends on the selected RRI. It is an integer value, drawn uniformly at random in the interval $\{\lceil 5 \cdot C \rceil, \ldots, \lfloor 15 \cdot C \rfloor\}$.[1] The quantity C is computed as follows:

$$C = \max\left\{1, \min\left\{5, \frac{\text{RRI}_{\text{th}}}{\text{RRI}}\right\}\right\}, \tag{1}$$

where $\text{RRI}_{\text{th}} = 100$ ms. The mean value of RC, denoted with $\overline{RC}$ is therefore given by $\overline{RC} = 10 \cdot C$, with $C \geq 1$.

[1] The notation $\lceil x \rceil$ and $\lfloor x \rfloor$ correspond to ceiling and floor functions of x, i.e., to the smallest integer not smaller than x and to the largest integer not larger than x, respectively.

In the case of standard SPS the mean number of times that a same SC is consecutively kept with a given period RRI is given by:

$$\eta_{\text{SPS}} = \frac{\overline{\text{RC}}}{1-P}, \tag{2}$$

where $\overline{\text{RC}}$ denotes the average of the RC, according to SPS settings.

B. DYNAMIC SCHEDULING (DS)

The DS resource allocation mechanism in 5G NR-V2X is defined in the standard [6]. With DS, a User Equipment (UE) dynamically selects resources for each individual transmission, without persistence. This means that after each transmission, the UE reselects a new resource for the next transmission, ensuring randomness. DS can be implemented setting the two parameters RC and P to fixed values as follows: RC $= 1$, $P = 0$. This setting guarantees that a selected SC is only kept once and then a new SC is reselected randomly over the set of all available SCs in the selection window. Note that monitoring the sensing window, to make the list of available resources, is only needed in a mixed environment where DS is used along with SPS.

DS is highly adaptable to varying traffic patterns and channel conditions, optimizing resource usage in scenarios where transmissions are sporadic or event-triggered. It is expected that DS offers inferior performance in case of periodic message flows, with respect to persistent scheduling. In fact, this has been assessed through extensive simulations in [21]. We will see however that DS can outperform persistent scheduling under the lenses of AoI-related metrics.

C. GEOMETRIC SEMI-PERSISTENT SCHEDULING (G-SPS)

G-SPS **is not** a novel resource allocation algorithm; rather, it offers an **alternative approach** for implementing persistence compared to the currently standardized SPS.

In G-SPS, persistence is realized by relying on a simple memoryless mechanism, where a node decides: (i) to keep the same SC it has been using with period RRI for one more period with probability $1-q$; or (ii) to jump to another SC to be reselected with probability q. Implementing this type of persistence is extremely simple. It relies on a single parameter, and the node does not need to store a counter or maintain a state other than the identity of the currently used SC and the period RRI. Exploiting standardized parameters, G-SPS can be practically implemented just setting RC $=$ 1 and $P = 1-q$.[2]

The probability distribution of the number of consecutive uses of the same SC with period RRI is Geometric. The probability of using the same SC h times is $(1-q)^{h-1}q$, $h \geq 1$.

We also define the variable η as the mean number of times the same SC is used consecutively. It is easy to verify that,

[2]In G-SPS we remove the constraint $P \in [0; 0.8]$ imposed by the standard.

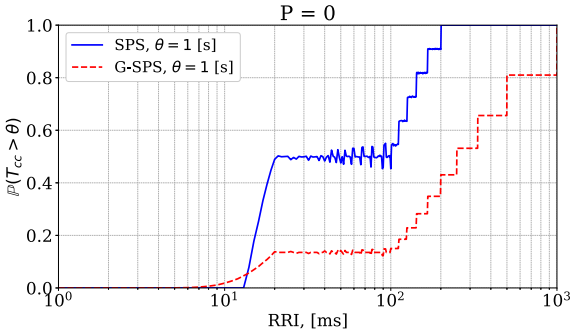

FIGURE 1. Probability that continued collision time T_{cc} between two nodes selecting the same SC lasts more than θ for $\theta = 1$ sec and $P = 0$. Comparison between standard SPS (blue solid line) and G-SPS (red dashed line).

in case of G-SPS, we have

$$\eta_{\text{G-SPS}} = \frac{1}{q}. \tag{3}$$

When comparing G-SPS with SPS, *we set the parameter q so that $\eta_{G\text{-}SPS} = \eta_{SPS} = \eta$ for a given value of η.*

The definition of G-SPS offers several advantages:

1) It extends the range of achievable persistence beyond the limitations of the current standard SPS settings (see Section III-D).
2) It improves tail properties of persistence, reducing the impact of persistence on re-iterated collisions (see Figure 1 below and comments thereof).
3) It simplifies the implementation of resource allocation algorithm compared to standard SPS, as it requires configuring only a single parameter.
4) Within the parameter ranges where both standard SPS and G-SPS are defined, G-SPS delivers nearly same performance as SPS, making it an effective replacement of SPS persistence mechanisms.
5) G-SPS allows setting the persistence level so as to minimize the AoI under periodic traffic conditions. This optimal setting cannot be achieved by the current standard SPS or DS.

As for the second point above, Figure 1 shows the probability that two nodes choose the same SC and both keep using it for at least a time θ. This is the probability of continued collisions for a time $T_{\text{cc}} > \theta$, conditional on two nodes colliding in their resource selection. The continuing collision stems from persistence. The effect is a prolonged gap between updates from the two nodes involved in the SC collision event.

Figure 1 plots $\mathcal{P}(T_{\text{cc}} > \theta)$ as a function of RRI, in case of $\theta = 1$ s and $P = 0$. When comparing SPS and G-SPS, the parameter q of G-SPS is set so that the values of η given by Equations (2) and (3) be the same.

It is evident that the tail of the probability distribution of the number of times that a specific SC is persistently used makes a difference. G-SPS and SPS are configured so as to have the same value of the *mean* value of the number of times that the

TABLE 2. Classification of persistence types.

Index	η	Persistence Class	Standard	Proposed
0	1	No persistence	DS	–
1	$(1, 10)$	Weak	–	G-SPS
2	$[10, 50)$	Moderate	SPS ($C = 1$)	G-SPS
3	$[50, \infty)$	Strong	–	G-SPS

same SC is used consecutively. However, G-SPS exhibits a *lighter* tail, resulting in significantly smaller probabilities of prolonged collision. For example, for RRI ranging between 20–100 ms, the probability that T_{cc} exceeds $\theta = 1$ s is about 0.14 for G-SPS, compared with 0.5 in case of SPS.

D. PERSISTENCE CLASSIFICATION

We introduce a persistence classification based on the variable η, the mean number of times that the same SC is used consecutively (see Equations (2)) and (3). The classification of *persistence types* is shown in Table 2.

In particular, four categories of persistence are identified, labeled with indexes between 0 and 3. Index 0 corresponds to DS, where there is **no persistence** at all.

The current SPS mechanism parametrization, with RC $\in \{5, \ldots, 15\}$ (in case $C = 1$) and $P \in [0; 0.8]$ falls inside the Index 2 category, namely, **moderate persistence**.

The other two categories extend persistence to ranges not achievable according to the standard. Index 1 corresponds to **weak persistence**, ranging between DS and SPS. Index 3 category goes beyond the maximum persistence allowed by SPS standard, namely **strong persistence**.

To establish the relationship between the proposed classification of persistence and the values of η attainable according to the current standard, Figure 2 shows the values of η as a function of RRI. The middle colored area corresponds to values obtainable according to standardized setting of SPS parameters RC and P. The horizontal dashed lines mark the borders between different regions of persistence, according to the proposed classification, each region corresponding to a horizonal band, from weak persistence in the lowest band, up to strong persistence in the upmost band. The vertical dashed line separates the range RRI $\geq$ RRI$_{\text{th}}$ = 100 ms, where it is $C = 1$, on the right, from the range RRI $<$ RRI$_{\text{th}}$ = 100 ms, where it is $1 < C \leq 5$, on the left.

It is evident that SPS can only provide moderate persistence as long as $C = 1$. Strong persistence is partially achievable for values of RRI less than 100 ms. Weak persistence is never attainable according to the standard. In Section VII, we will see numerical results which show that the minimum of AoI is attained in the weak persistence region, which is forbidden for standard-compliant parametrization.

IV. KEY PERFORMANCE METRICS

This section focuses on the key metrics relevant to our analysis. The 3GPP standard [11] introduces a set of performance metrics to evaluate the reliability and timeliness of NR-V2X communications. We review those metrics,

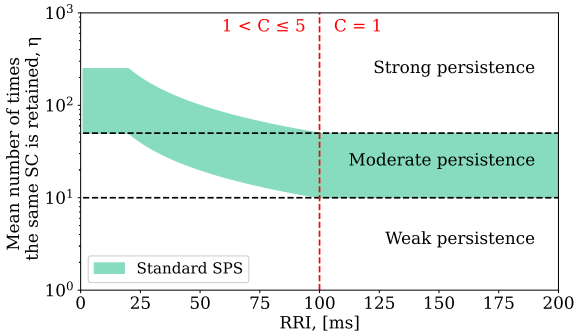

FIGURE 2. Values of η as a function of the RRI. The colored area corresponds to values of η that can be obtained with the standardized SPS. The horizontal lines mark the borders of the three persistence regions (horizontal bands) identified by indexes 1 to 3. The vertical dashed line marks the RRI threshold RRI$_{\text{th}}$ = 100 ms. The RRI values to the right of this line result in $C = 1$. The values to the left of this line correspond to $1 < C \leq 5$.

introduce more, and provide details on how they are estimated from simulation traces. Additionally, in this section we demonstrate the difference between the AoI metric and the standardized metrics of PRR and PIR, and prove its importance for 5G NR-V2X sidelink scenario analysis.

A. STANDARDIZED METRICS

1) PACKET RECEPTION RATIO (PRR)

For broadcast communications, PRR (referred to in the standard [11] as PRR type 1) measures the success ratio of packet transmissions.

PRR for each transmitted packet, say packet j, and for a given distance range $[a, b]$ is defined as:

$$\text{PRR}_j = \frac{O_j}{H_j}, \tag{4}$$

where

- O_j is the number of nodes that decode the considered packet j and lie at a distance between a and b from the transmitting node.
- H_j is the overall number of nodes lying at a distance between a and b from the transmitting node.

Over a simulation generating M packets, the average PRR is computed as a weighted average of individual PRR values:

$$\text{E[PRR]} = \sum_{j=1}^{M} \frac{H_j}{\sum_{i=1}^{M} H_i} \cdot \text{PRR}_j = \frac{\sum_{j=1}^{M} O_j}{\sum_{j=1}^{M} H_j}. \tag{5}$$

In the simulation experiment, the values $a = i \cdot 50$ m, $b = (i+1) \cdot 50$ m are considered for $i = 0, 1, \ldots, 20$, that is up to 1 km.

2) PACKET INTER-RECEPTION (PIR)

The PIR [11][3] quantifies the time between two consecutive successful receptions of messages belonging to the same

[3]The term Peak Age of Information (PAoI) is also commonly used in the literature and is entirely equivalent to PIR.

application flow. More in depth, let us consider the local dynamic map of a node j, where data collected from neighboring nodes is collected. Let $t_{ij}(k)$ be the delivery time of an update at node j from node i, where $k \geq 2$ is index of received packet. Let $A_{ij}(t)$ denote the age of the information stored at j and coming from node i at time t. It is $A_{ij}(t) = t - t_{ij}(k-1)$ for $t \in [t_{ij}(k-1), t_{ij}(k))$. Then, by definition, the *peak* AoI is given by

$$Y_{ij}(k) = \sup_{t \in [t_{ij}(k-1), t_{ij}(k))} A_{ij}(t) = t_{ij}(k) - t_{ij}(k-1). \quad (6)$$

Let u_{ij} the number of updates delivered to j by node i. The average PIR is obtained as

$$\mathrm{E}[\mathrm{PIR}_{ij}] = \frac{1}{u_{ij}} \sum_{k=1}^{u_{ij}} Y_{ij}(k). \quad (7)$$

Note that each peak is weighted the same in this average, no matter how large it is.

The average PIR at node j, encompassing information flows that node j receives from all its neighbors, is obtained by means of a weighted average:

$$\mathrm{E}[\mathrm{PIR}_j] = \sum_{i \in \mathcal{N}_j} \frac{u_{ij}}{\sum_{k \in \mathcal{N}_j} u_{kj}} \mathrm{E}[\mathrm{PIR}_{ij}], \quad (8)$$

where $\mathcal{N}_j$ is the set of all nodes from which at least X messages have been successfully delivered to j. In the evaluation of simulation experiments, we set $X = 2$. Obviously, this average can be evaluated only for nodes for which $\mathcal{N}_j \neq \emptyset$.

Analogously, the overall PIR is obtained through a weights average of the $\mathrm{E}[\mathrm{PIR}_j]$ for all j.

PIR focuses on the worst-case scenario, representing the maximum staleness experienced between consecutive updates.

B. NON-STANDARDIZED METRICS

1) CLR & PLR

To assess the reliability of communication over a given distance range $[a, b]$, two complementary metrics are used: the CLR and PLR. These metrics quantify the specific impact of collisions and poor propagation conditions, respectively (see Section V for specifications on how the simulation model identifies these two root causes of failed packet reception).

CLR reflects the proportion of packets lost due to collisions:

$$\mathrm{CLR} = \frac{N_{\mathrm{CL}}}{N_{\mathrm{PL}} + N_{\mathrm{CL}} + N_{\mathrm{SR}}}, \quad (9)$$

where N_{CL} is the number of packets lost in collisions, N_{PL} represents packets lost due to poor propagation conditions, and N_{SR} is the number of successfully received packets.

PLR measures the fraction of packets lost due to insufficient Signal-to-Noise Ratio (SNR):

$$\mathrm{PLR} = \frac{N_{\mathrm{PL}}}{N_{\mathrm{PL}} + N_{\mathrm{CL}} + N_{\mathrm{SR}}}. \quad (10)$$

TABLE 3. Simulation parameters.

Parameter	Values
Highway length, L	5000 m
Vehicle density, ρ	35, 70, 100, and 140 veh/km
Maximal vehicle density, ρ_{max}	154 veh/km
Number of lanes	6
Vehicle speed	70 km/h
Channel bandwidth, BW	10 MHz
OFDM numerology, μ	0
Sub-Carrier Spacing, B_{sc}	15 kHz
Time slot duration, T_s	1 ms
Modulation and Coding Scheme (MCS)	MCS13
Modulation	16 QAM
Code rate	0.4875
# of RBs per Sub-Channel	50, 25, 10
# of Sub-Channels per time slot, n_{SC}	1, 2, 5
RRI	100 ms, 50 ms, 20 ms
Message generation time, T_{gen}	= RRI
Transmission power	23 dBm
RSRP threshold	−120.07 dBm
Noise figure	9 dB
Margin for idle/busy channel assessment	3 dB
SC re-selection back-off factor	3 dB

These metrics provide a detailed view of the distinct challenges posed by physical layer conditions and network contention.

2) AGE OF INFORMATION (AOI)

AoI is an application-level metric that can be applied across a wide range of applications (e.g., cooperative awareness, cooperative perception, maneuver coordination), regardless of their specific nature or domain. AoI measures the freshness of the most recent information received from a transmitting source. The average value of AoI for messages sent by node i and collected by node j is computed as follows:

$$\mathrm{E}[\mathrm{AoI}_{ij}] = \lim_{T \to \infty} \frac{1}{T} \int_0^T A_{ij}(t)\, dt \approx \frac{\sum_{k=1}^{u_{ij}} \frac{1}{2} Y_{ij}^2(k)}{\sum_{k=1}^{u_{ij}} Y_{ij}(k)}, \quad (11)$$

where we recall that u_{ij} is the number of successful updates sent by node i and received by node j, and $Y_{ij}(k) = t_{ij}(k) - t_{ij}(k-1)$. There is a strict connection between the average AoI and PIR. Specifically, it is

$$\mathrm{E}[\mathrm{AoI}] = \frac{\mathrm{E}[\mathrm{PIR}^2]}{2 \cdot \mathrm{E}[\mathrm{PIR}]}. \quad (12)$$

AoI for all information flows collected at node j and the overall AoI of the system can be obtained with averaging similar to those defined with PIR. We also consider extreme values of AoI by evaluating quantiles. The quantile q (e.g., $q = 90$) is evaluated as the threshold AoI_q such that $\mathcal{P}(\mathrm{AoI} \leq \mathrm{AoI}_q) = q/100$, i.e., it is that value which is not exceeded with probability $q/100$ (e.g., probability 0.9 in case $q = 90$). This metric provides critical insights into the timeliness of data updates, which is essential for safety-critical vehicular applications.

The PIR metric is an averaged estimate of AoI peaks, which does not account for the duration of vehicles being in a collision state. For instance, Figure 3 illustrates the plot of a sample path of AoI for a sequence of update delivery, most

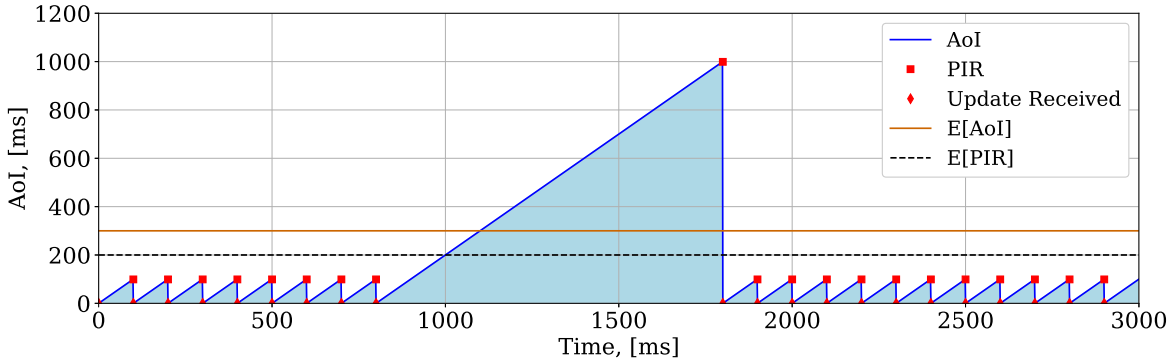

FIGURE 3. PIR and AoI sample path example.

of which are delivered timely, with short time gaps between consecutive updates, except of one, which corresponds to a relatively long time, where no successful update is received.

The time-averaged AoI and the average PIR are shown as a solid line and dashed lines, respectively. It is evident that the time-averaged AoI (formally defined in Equations 11) is *greater* than the average PIR. The reason is that the single large peak of AoI has a unit weight as all other peaks in the evaluation of average PIR. On the contrary, in the time averaged AoI, the full time behavior of the age function is considered, hence a large peak weights more just by virtue of the corresponding large duration.

From the perspective of safety-critical applications, the large time gap between two consecutive updates (e.g., due to a row of collision events) could lead to dangerous situations on the road, giving rise to a sort of "blind spot" that makes the node sending updates invisible to its neighbor for the duration of the time gap.

From a statistical perspective, AoI and PIR capture different characteristics of information freshness. AoI provides a continuous measure, offering insight into the average freshness of information over time. It is well-suited for evaluating long-term performance and can be analyzed using metrics like mean AoI, which reflects the overall timeliness of updates. AoI can reveal additional critical information about the system's performance, while PIR remains essential for understanding the worst-case scenarios. For these reasons, we advocate for extending the standard to include AoI alongside PIR.

V. SIMULATION SETUP

This section describes the simulation model used in the performance evaluation. The model was implemented in ns-3 using the open-source MoReV2X module developed for the simulation of NR-V2X Mode 2 [50], [51]. The numerical values of the main simulation parameters are listed in Table 3.

The considered scenario represents a 5000 m-long highway with three lanes in each direction, where vehicles travel at an average speed of 70 km/h. Assuming an average vehicle length $\ell = 10$ m, a reaction time $\tau = 0.5$ s, and a maximum deceleration of leader and follower vehicles equal to $a_l = g = 9.8\,\text{m/s}^2$ and $a_f = g/2$, respectively, the minimum spacing between consecutive vehicles on the same lane is $\Delta = \ell + \tau v + v^2(1/a_f - 1/a_l)/2 \approx 37$ m. Hence, the maximum vehicle density on the six lane road is 154 veh/km. We consider a baseline vehicle density of 140 veh/km, which represents approximately 90 % of the maximum achievable density, indicating a high traffic load. To assess the impact of traffic conditions, we conduct additional simulations under varying vehicle densities. The evaluated densities are $\rho =$ 140, 100, 70, and 35 veh/km.

Each vehicle generates a periodic stream of messages, broadcast through the sidelink channel. Messages are generated with a period equal to the RRI.

As for the radio interface, NR-V2X radios operate in a 10 MHz channel within the 5.9 GHz ITS band. Each Resource Block (RB) comprises 12 sub-carriers and 14 symbols. Part of symbols are devoted to physical layer functions (e.g., pilot tones), the remaining ones are used to support SCs, comprising Sidelink Control Information (SCI), organized in so called two stages, and a Transport Block (TB). The detailed symbol allocation is specified in the standard and summarized, as concerns the considered simulation model, in [52].

We consider three different configurations of the sidelink channel by setting the number of SCs per slot n_{SC} to 1, 2, and 5. Correspondingly, the number of RB assigned to a SC is 50, 25 and 10. Two of those SCs are used by the SCI stage 1. The MCS 13 is selected, using 16-QAM modulation (modulation order $q = 4$) and coding rate $r = 0.4875$. By accounting for the details of symbol allocation, the resulting data payload size of the corresponding TBs are 1473 Byte for 1 SC per slot, 528 Byte for 2 SCs per slot, and 217 Byte for 5 SCs per slot. These values were obtained using the link-level simulator described in [52].

The selection window for the multiple access procedure is identified with a time span equal to one RRI. Hence, the available number of SCs for node selection is $K = n_{\text{SC}} \lfloor \frac{\text{RRI}}{T_s} \rfloor$, where T_s denotes the duration of a slot and n_{SC} is the number of SCs per slot. To maintain the same value of K for the different sidelink channel configurations, the RRI is set to $100\,\text{ms}/n_{\text{SC}}$. This scaling maintains the proportion between

TABLE 4. Comparison between G-SPS and previously reported works.

Reference	RC	P	η	Persistence Class Index	Assumptions	Metrics
Rolich et al. [7]	1 or [5;15]	[0;0.95] or [0;0.8]	[2;50]	1-3	No hidden nodes, no SC reuse, no propagation losses, periodic traffic	PRR, PIR, AoI
Rolich et al. [8]	1 or [5;15]	[0;0.99] or [0;0.8]	[1;1000]	0-3	No hidden nodes, no SC reuse, highway propagation, periodic traffic	PRR, CLR, PLR, PIR, AoI
Lusvarghi et al. [20]	[1;10]	0	5	1	Hidden nodes, SC reuse, suburban propagation, mixed traffic	PRR, CLR, PLR, PIR
Lusvarghi et al. [21]	1 or [5;15]	1 or 10	1 or 10	0,2	Hidden nodes, SC reuse, highway propagation, periodic, aperiodic and mixed traffic	PRR, CLR
Chourasia et al. [23]	[2;7], [5;15], [10;30]	0, 0.4, 0.6, 0.8	[7,5; 50]	1,2	Hidden nodes, SC reuse, highway propagation, periodic traffic	PRR, PIR
Bazzi et al. [42]	[5;15]	0 or 0.8	10 or 50	2	Hidden nodes, SC reuse, highway propagation, periodic traffic	PRR
Bazzi et al. [43]	[5;15]	[0;0.8]	[10; 50]	2	Hidden nodes, SC reuse, urban and highway propagation, periodic traffic	PRR
Yoon et al. [44]	[5;15]	0 or 0.8	10 or 50	2	Hidden nodes, SC reuse, highway propagation, aperiodic traffic	PRR
Cao et al. [45]	[5;15]	[0.1;0.7]	[11.11;33.33]	2	Hidden nodes, SC reuse, highway propagation, periodic traffic	CLR, PIR
Cao et al. [46]	[5;15]	0.5	[500;1500]	3	Hidden nodes, SC reuse, highway propagation, periodic traffic	PRR, CLR
Djaidja et al. [47]	[1;15]	[0;0.8]	[8;50]	0-2	Hidden nodes, SC reuse, highway propagation, periodic traffic	PRR
Rolich et al. [48]	1 or [5;15]	0 or [0;0.8]	1 or [10;50]	0,2	No hidden nodes, no SC reuse, no propagation losses, periodic traffic	AoI
Rolich et al. [49]	1 or [5;15]	[0;0.995] or [0;0.8]	[1;200]	0-3	Hidden nodes, SC reuse, no propagation loss, periodic traffic	Probability of AoI violation, reuse order
This paper	1	[0,0.999]	[1;1000]	0-3	Hidden nodes, SC reuse, highway propagation, periodic traffic	PRR, CLR, PLR, PIR, AoI, AoI quantiles

the amount of messages generated by vehicle population per unit time and the amount of available resources in a selection window (which is anyway equal to one RRI).

The transmission power level is set to 23 dBm. Background noise power is $P_N = k_B T_0 N_F B$, where k_B is Boltzmann's constant, T_0 is the receiver temperature, N_F is the receiver noise figure, and B is the bandwidth. Letting $T_0 = 300\,\text{K}$, $N_F = 9\,\text{dB}$, and $B = n_{\text{RB}} \cdot 180\,\text{kHz}$, we have $P_N = 10\log_{10} n_{\text{RB}} - 112.3\,\text{dBm}$. In the three considered SC configurations we have $n_{\text{RB}} = 50, 25, 10$, so it is $P_N = -95.3\,\text{dBm}$, $-98.3\,\text{dBm}$, and $-102.3\,\text{dBm}$, respectively.

Path loss and shadowing effects are modeled using the approach from [11], while fast fading is accounted for by incorporating Block-Error Rate (BLER) curves from [52]. The WBS effect [42] is also considered.

In the simulation, information decoding in a SC is structured as follows. For each transmission link between transmitting node i and receiving node j, where i transmits on a given SC s and j listens to that SC, the SNR and Signal-to-Noise-plus-Interference Ratio (SNIR) are computed.[4] Noise power is computed as detailed above. Channel gain is computed based on the distance between nodes i and j and according to the path loss model specified in [11]. The interference is the sum received power of all transmissions of nodes $\neq i$, using the same SC s. The obtained values of SNR and SNIR are then used as input values to the BLER curve (implemented as a table in the simulator). Let P_{SNR} and P_{SNIR} be the two obtained output values, respectively. The TB carried in the considered SC s, transmitted by node i, is considered to be lost to the receiving node j, because of propagation effect, with probability P_{SNR}. If that is not the case, then the TB is considered to be lost to receiving node j, because of collision effect, with probability P_{SNIR}. If that is not the case either, then the TB is considered to have been successfully received at node j.

As for sensing, the noise floor on a single sub-carrier is given by Reference Signal Receive Power (RSRP). RSRP $= k_B T_0 N_F B_{\text{sc}}$, where k_B is Boltzmann's constant, T_0 is the receiver temperature, N_F is the receiver noise figure, and B_{sc} is the sub-carrier spacing, depending on the numerology. A sub-carrier is deemed to be busy if the received power level exceeds this noise floor level by a margin M. Letting $M = 3\,\text{dB}$ and $N_F = 9\,\text{dB}$, it is found that the RSRP threshold

[4]This implies that node j does not transmit on a SC in the same slot as SC s.

is −120.07 dBm. At time of SC (re)selection in the Medium Access Control (MAC) sublayer, the initial threshold is set to the obtained RSRP, and the back-off factor is fixed at 3 dB. The target minimum fraction of SCs in a selection window that must be declared idle is set to 20 %. If less than that fraction of SCs in the re-selection window are declared to be idle, the RSRP threshold is scaled by the back-off factor (increased by that amount of dB) and SC assessment is repeated.

The simulated DS and SPS algorithms are fully compliant with the standard. Since we choose values of RRI $\leq$ 100 ms, it follows that $C = 1$ and RC is drawn uniformly at random from the integer set between 5 and 15, while P ranges between 0 and 0.8. Consequently, the parameter η ranges between 10 and 50 for SPS. DS corresponds to persistence class Index 0, with the parameter $\eta = 1$.

G-SPS has also been implemented in the simulator with a configuration of $RC = 1$ and $P \in [0, 1)$, thereby enabling coverage of the entire range of persistence values (Index 1, 2, and 3), as detailed in Section III and Table 2. In this configuration, the parameter η can take any value > 1.

Table 4 compares our proposed approach of defining persistence using G-SPS with previously reported works in Section II, highlighting the values of the key persistence parameters (RC, P, η) adopted in the simulations, the corresponding persistence class from our classification (Section III-D), as well as the underlying assumptions and performance metrics. The table shows that most prior studies were restricted to a narrow persistence range – typically the moderate, as it aligns with the standard SPS – whereas the present work, through the proposed G-SPS approach, investigates the full persistence range under periodic traffic, realistic propagation models, hidden nodes, and scenarios enabling spatial reuse of SCs. It supports the novelty of our contribution.

VI. INTEGRITY PERFORMANCE

In the context of C-V2X, integrity refers to the reliable delivery of messages from the source node to its neighbors. The primary performance metric for evaluating integrity is the PRR. In this section, we highlight the superior integrity performance of the SPS mechanism compared to DS and analyze the impact of different persistence classes on PRR.

Persistence is defined as the average number of consecutive transmissions in which the same SC is retained for a given RRI, η, as specified in Equations (2) and (3). In Figure 4, DS corresponds to $\eta = 1$, while weak, moderate, and strong persistence are represented by $\eta = 2$, $\eta = 20$, and $\eta = 200$, respectively. These values were selected as representative samples, with η increased by one order of magnitude across classes (2, 20, 200), to highlight the differences in PRR and CLR performance at varying persistence levels. The full range of η values is illustrated in Figure 5.

Figure 4a illustrates the PRR as a function of the distance between transmitter and receiver for each persistence class

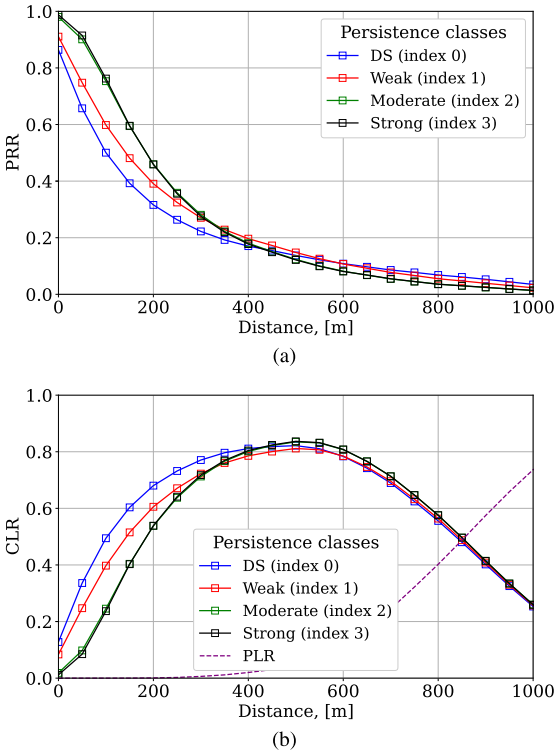

FIGURE 4. PRR (a) and CLR, PLR (b) as a function of distance between transmitter and receiver. In this figure, DS corresponds to $\eta = 1$, with weak persistence defined by $\eta = 2$, moderate persistence by $\eta = 20$, and strong persistence by $\eta = 200$.

described in the Section III, while Figure 4b shows the CLR and PLR.

As shown in Figure 4a, the best PRR performance is demonstrated by the moderate (Index 2) and strong persistence (Index 3) classes, while DS (Index 0) yields the worst results. The main reason is that, when the system exhibits higher persistence, the frequency of potential SC changes is significantly reduced, resulting in fewer collisions. At the same time, we observe that the PRR value decreases monotonically due to collisions and signal attenuation and propagation losses as the communication path distance increases. It is important to note that high message reliability (PRR above 90 %) is unattainable with DS, it is reached up to a distance of 20 m for weak persistence (Index 1), and up to 50 m for moderate and strong persistence. When the distance falls within the 400 m range, the average probability of successful message delivery drops to around 20 %. Beyond that range it is essentially negligible, with the considered parameter setting.

However, even at relatively short distances, packet losses can still occur due to collisions. Figure 4b presents a breakdown of the packet loss probability, defined as 1 − PRR, into two contributing factors: losses due to collisions, quantified by the CLR, and losses resulting from insufficient received signal strength, represented by the PLR. In the figure, CLR is depicted using solid lines, while PLR is shown with dashed lines. At very short distances (a few tens of meters),

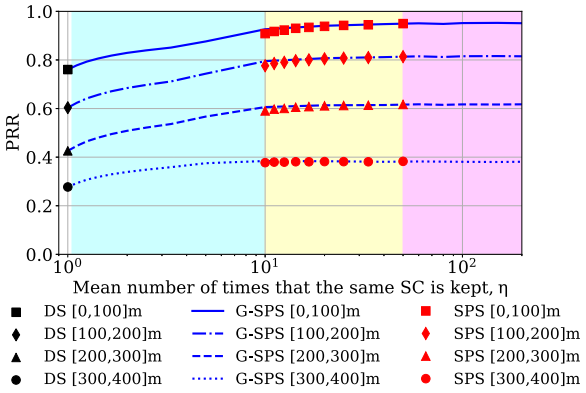

FIGURE 5. PRR versus mean times the same SC is kept (η) for a vehicle density of 140 veh/km and 1 SC, with persistence classes highlighted: weak (green area), moderate (yellow area), and strong (red area). Line curves are obtained with G-SPS, while markers correspond to DS (black square marker) and SPS (red markers).

the signal strength is sufficient to mitigate interference effectively. However, a high vehicle density combined with elevated transmitter power results in a substantial number of collisions. This is primarily due to nodes selecting the same SCs simultaneously and the increased interference associated with spatial reuse of radio resources. A distinct trend emerges: for inter-vehicle distances up to 400 meters, DS (Index 0) and weak persistence (Index 2) lead to a higher number of collisions, as expected. In contrast, at short distances, signal attenuation has minimal impact, becoming a significant factor only at distances exceeding 600 m.

In Figure 5, values of PRR averaged over several different distance ranges are plotted as a function of η. The persistence classes are highlighted by background coloring. The colored area on the left (green) corresponds to weak persistence. The central colored stripe (yellow) corresponds to moderate persistence. Strong persistence is highlighted by the right-most colored area (red). Blue line plots are obtained by using G-SPS. Markers refer to standard mechanisms: DS is shown with a black square marker ($\eta = 1$), while SPS is shown by red markers. The plot displays four line and marker combinations, each representing a specific range of distances: [0, 100] m, [100, 200] m, [200, 300] m, and [300, 400] m.

The monotonic increase in the probability of successful message delivery is observed as persistence increases. At the same time, we observe that the standard SPS outperforms DS and G-SPS with weak persistence in all cases. Essentially no further performance gain is obtained by pushing persistence into the strong persistence region. It is worth emphasizing that the proposed G-SPS (blue line) exhibits identical performance to the standardized SPS (red markers), confirming the consistency of the proposed approach.

Figure 6 presents an analysis of the PRR as a function of persistence under G-SPS, considering varying vehicle densities ranging from 35 veh/km to 140 veh/km and 1 SC with 50 RBs. The evaluation is conducted across two distinct distance intervals: [0, 250] m and [250, 500] m.

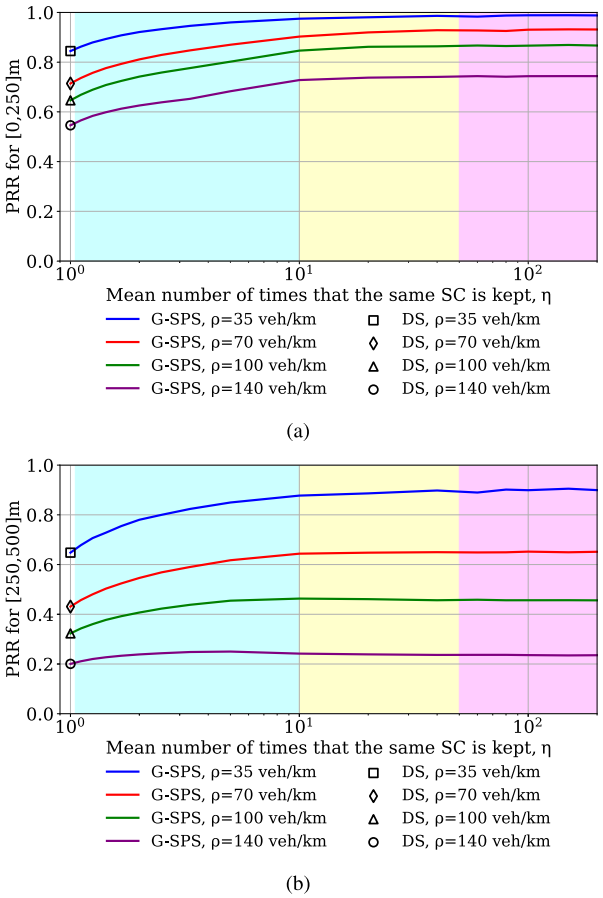

FIGURE 6. PRR obtained with G-SPS as a function of the mean time the same SC is kept (η) for four different vehicle densities, with persistence classes highlighted: weak (green area), moderate (yellow area), and strong (red area). The two subplots correspond to different distance ranges: (a) [0,250] m and (b) [250,500] m.

As expected, an increase in vehicle density negatively impacts PRR performance due to a higher probability of packet collisions. However, a quantitative analysis reveals that for short distances (up to 250 m), the PRR variation remains limited to approximately 10 %. For distances up to 500 m, the variation increases to around 20 %. Notably, reaching moderate persistence, the PRR stabilizes at higher values across all density levels diminishing the impact of collisions. Furthermore, the results confirm that PRR improves monotonically with persistence, suggesting that higher persistence benefits PRR. However, the observed improvements are relatively modest, indicating that beyond a certain threshold, additional persistence yields diminishing returns in mitigating packet loss.

Figure 7 presents an alternative perspective, where the vehicle density is fixed at 140 veh/km, while varying the number of allocated SCs (1, 2, and 5). This analysis aims to demonstrate that, under the given simulation configuration, different channel configurations exhibit nearly identical performance due to the extreme similarity in BLER curves. However, it is important to note that for alternative

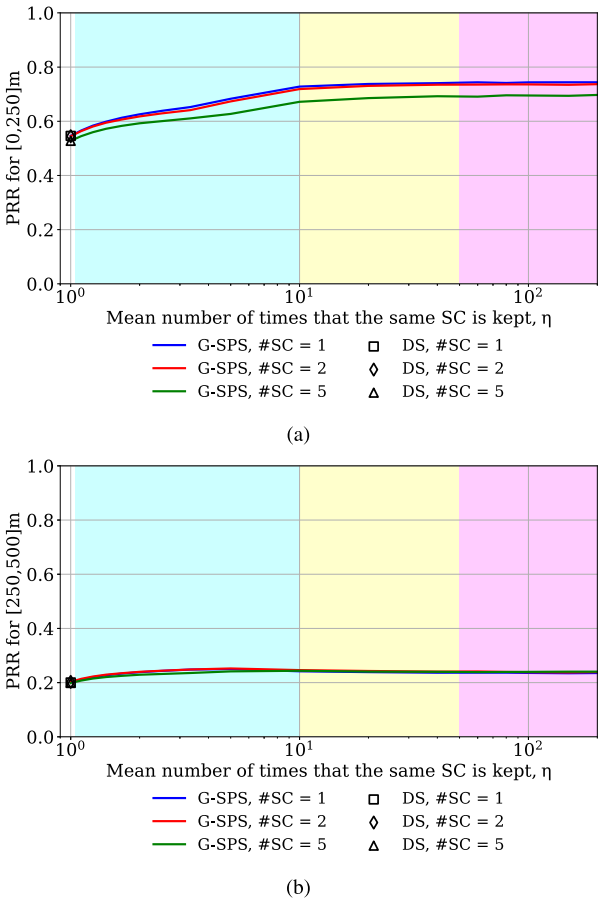

FIGURE 7. PRR obtained with G-SPS as a function of the mean time the same SC is kept (η) for three different SC configurations, with persistence classes highlighted: weak (green area), moderate (yellow area), and strong (red area). The two subplots represent different distance ranges: (a) [0,250] m and (b) [250,500] m.

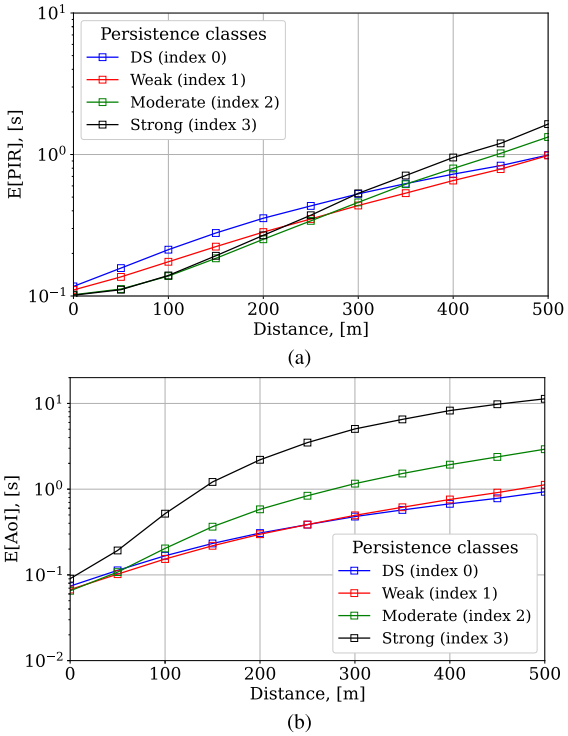

FIGURE 8. Mean PIR(a) and AoI(b) as a function of the distance between transmitter and receiver. In this plot DS corresponds to $\eta = 1$, with weak persistence defined as $\eta = 2$, moderate persistence as $\eta = 20$, and strong persistence as $\eta = 200$.

numerology and MCS configurations, the results may deviate more significantly, as these factors can exert a stronger influence on BLER curves, leading to substantial performance differences across channel configurations. Similar to the analysis with varying vehicle densities, we examine two distance intervals: [0, 250] m and [250, 500] m. For short distances, we observe minor differences in PRR performance depending on the number of SCs; however, these differences remain negligible and follow the same behavioral trend as previously noted. At longer distances, the PRR values for all channel configurations converge, indicating no significant variation in performance.

The evaluation of different traffic flow densities and channel configurations reinforces the generality of our findings. The results suggest that our conclusions are not limited to a specific scenario but can be extended to other configurations, highlighting the robustness and scalability of the proposed approach.

VII. TIMELINESS PERFORMANCE

This section explores the timeliness of data delivery for periodic update message flows, comparing SPS, DS and G-SPS approaches. Since freshness of information is the focus, the considered key performance indicators are PIR and AoI, defined in Section IV.

A. DISTANCE-DEPENDENT ANALYSIS

In this section, we evaluate PIR and AoI as a function of distance between transmitter and receiver.

Figures 8a and 8b show the average PIR and AoI as a function of distance for the persistence classes defined in Section III. In these plots, DS corresponds to $\eta = 1$, while weak, moderate, and strong persistence are represented by $\eta = 2$, $\eta = 20$, and $\eta = 200$, respectively. These representative values, chosen by increasing η one order of magnitude across classes, highlight the contrasting effects of persistence on system performance. Results for the full range of η values are reported in Figure 9.

In our analysis of PIR and AoI for a vehicle density of $\rho = 140$ veh/km, we limit the scope up to 500 m, as vehicles are generally unable to communicate effectively beyond this distance, and timely communication with nearby neighbors is more critical in practice.

Figure 8a illustrates the PIR, which quantifies the average time interval between two consecutive successfully received messages between a pair of vehicles. As expected, the average PIR increases with the distance between the transmitting and receiving vehicles, as the probability of successful reception decreases due to fading and collisions. However, it is crucial

to highlight that the overall trend closely mirrors that of PRR: at short distances, moderate and strong persistence yield the best performance. In the range of 250–350 meters, the lines intersect, suggesting that as the distance increases, higher persistence becomes slightly less effective compared to more randomized weak persistence and DS. The increase in PIR with strong persistence is attributed to prolonged collision states—when a collision occurs, the involved nodes persist in the collision scenario for an extended duration, leading to delays in successful message reception.

This phenomenon becomes even more pronounced when analyzing the AoI, as shown in the Figure 8b. Unlike PIR, the AoI metric is more sensitive to the balance between the frequency and duration of collisions. Results in Figure 8b show that the worst performance is found for strong persistence, with a significant deterioration as compared to PIR. At the same time, also moderate persistence no longer delivers the best performance at any distance region, also showing a notable worsening relative to PIR. The best average AoI performance is achieved by DS and weak persistence.

We have previously observed this phenomenon in simpler scenarios [7], [8], explained by the need to maintain a balance between the frequency and duration of collisions. Persistence reduces the number of collisions, but significantly increases their duration, resulting in colliding vehicles remaining out of sight for longer periods of time. Stronger persistence appears to turn the communication channel among vehicles more and more into an on-off channel. As a result, *even if persistence improves PRR, it turns out to affect AoI adversely*. In fact, a larger number of message losses, but occurring randomly, seems to affect the timeliness of information less than sporadic, prolonged message losses in a row.

The findings of this section highlight the need for a deeper understanding of the potential to optimize persistence classes based on specific application requirements, balancing reliability and timeliness to support safety-critical vehicular communications.

B. PERSISTENCE-DEPENDENT ANALYSIS

In this section, we analyze the impact of different persistence classes on PIR, and AoI measured obtained by averaging over distance ranges. Persistence is expressed as η, i.e., the mean number of times the same SC is retained with a given RRI (see Equations (2) and (3)). The achievable persistence values for each persistence class are highlighted with colored zones: weak persistence is shown in the green zone, moderate persistence in the yellow zone, and strong persistence in the red zone.

In Figure 9, the mean values of PIR, and AoI are presented as a function of η. Red markers represent the performance of the standard SPS, which implements only the moderate persistence class. Blue lines correspond to G-SPS (described in Section III), covering weak, moderate, and strong persistence classes. Black markers indicate the performance of the standard DS. Four different combinations of lines and markers are used, corresponding to specific distance ranges: [0, 100] m, [100, 200] m, [200, 300] m, and [300, 400] m.

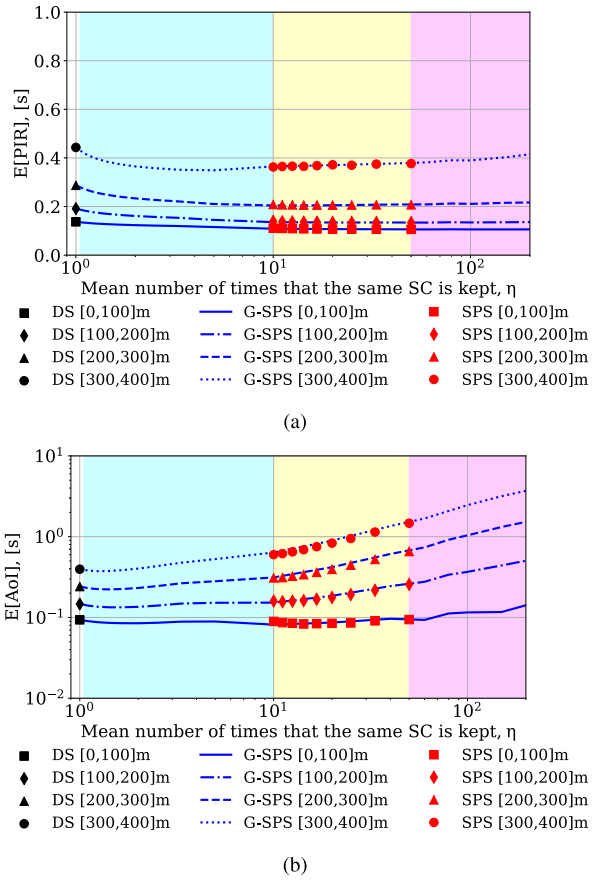

FIGURE 9. Mean PIR (a) and AoI (b) as a function of η.

The mean PIR values presented in Figure 9a exhibit stable behavior for distances below 300 m, reinforcing the conclusion that moderate persistence is the most effective strategy compared to other persistence types. This finding aligns with the results obtained in Section VII-A. However, for distances exceeding 300 m, we observe a shift in PIR behavior following the intersection of the curves in the figure. Beyond this point, weak persistence emerges as the most favorable choice for minimizing PIR. Notably, at these distances, fewer than 30 % of all packets are successfully delivered due to frequent collisions. This observation corroborates our results, demonstrating that lower persistence leads to improved performance by introducing a degree of randomization in packet losses, thereby reducing their overall duration.

Unlike PRR and PIR, the mean AoI is a non-monotonic function for all considered distances between transmitter and receiver, exhibiting a distinct persistence optimum. For distances greater than 100 m, the optimal persistence class is weak persistence, providing the best mean AoI performance. For shorter distances, the minimum mean AoI can be achieved with either weak or moderate persistence.

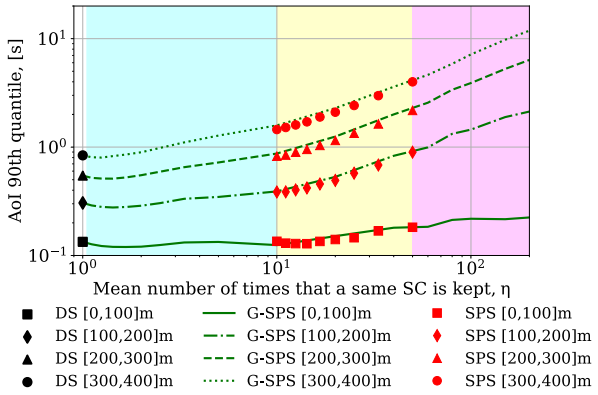

FIGURE 10. AoI 90th quantile as a function of η.

The presence of a minimum in all cases clarify our findings from Section VII-A, showing that weak persistence outperforms DS by effectively balancing the frequency and duration of collisions. Notably, as the distance increases, the minimum mean AoI shifts closer to the performance of DS. This indicates that reducing persistence is necessary to achieve optimal AoI as the distance grows.

When comparing the standardized algorithms (DS and SPS, we observe that for the short distance range (less than 100 m) DS matches SPS, but for larger distances DS outperforms SPS. This finding calls into question the opportunity for implementing the more complex SPS algorithm, given the simplicity and comparable performance of DS. The superiority of DS over SPS has previously been demonstrated for aperiodic traffic in [21]. Our analysis shows that, even in the case of periodic traffic (for which SPS is designed), the standard SPS can still underperform compared to DS.

The findings stemming from the analysis of the average AoI are further confirmed by the results shown in Figure 10, which shows the 90th quantile of AoI as a function of η.

First, it is important to highlight the presence of well-defined minima across all distance ranges, consistently located within the weak persistence zone. Second – and most critically – the choice of persistence class and its implementation should be directly aligned with the requirements of the specific application. For instance, if it is necessary to ensure that 90 % of vehicles data maintain an AoI below 1 s at distances up to 300 m, various options can be employed: moderate persistence (only partially), weak persistence, or DS. What is the best option to pursue can be identified by considering further specification. Simplicity of implementation and ease of parameter configuration is an important aspect, making DS preferable, provided that information freshness requirements are met. On the other hand, if the goal is to guarantee an AoI close to the standardized requirements [53] for 90 % of vehicles, only weak persistence with its optimal values can be relied upon.

To dig further into AoI performance, we consider the mean AoI of messages sent by node i and collected at another node j, denoted with $\mathrm{E}[A_{i\to j}]$. To visualize the values of $\mathrm{E}[A_{i\to j}]$ collected in a simulation for all pairs of vehicles we resort to a dispersion plot (also know as scatter plot). Each value $\mathrm{E}[A_{i\to j}]$ is reported as a dot, whose abscissa along the horizontal axis corresponds to $\mathrm{E}[A_{i\to j}]$. To make the dot cloud visible, each dot is displaced by a random amount along the vertical axis. This is just a visualization trick, with no special meaning otherwise.

Figure 11 shows dispersion plots of AoI for three different persistence settings and three different distance ranges (nine panels overall). The X-position of each point corresponds to the AoI value of one vehicle pair, and a random value along the Y-axis is used for better visualization. Note that only vehicle pairs (i, j) such that j receives at least two messages from i are considered. For each distance range, compared persistence settings correspond to: DS (blue points), SPS with $P = 0$ (red points); SPS with $P = 0.8$ (green points). The last two arrangements mark the boundaries between weak to moderate persistence, and moderate to strong persistence, respectively. The dashed black vertical lines mark the overall average AoI value for the cloud of points.

For each distance range, the ratio ϕ of the number of vehicle pairs that have at least two successful messages to the total number of vehicle pairs within the given distance range was calculated. The measured value of ϕ for each persistence setting and each distance range is reported within the plots. It turns out that it is the same for the three considered persistence distance in each distance range, while it decreases substantially as distance grows. For each given distance range, having the same ϕ for all persistence settings proves that their merit can be directly assessed by looking at offered AoI performance, given that effective connectivity is the same for all settings.

It should be noted that ϕ does not correlate with the PRR, as it only considers the presence of at least two successful transmissions, without accounting for the number of unsuccessful transmissions. This fact allows a deeper analysis of the impact of persistence on AoI.

As persistence increases, we observe an increase in the variability of AoI across different pairs, due to many message reception failures in a row because of persistent collision events. In case of DS, such a situation does not occur, since messages from node i to node j get lost randomly. Albeit the fraction of lost messages is higher with DS than with persistent algorithms (as proved by comparing PRR values of DS and SPS), message losses are scattered randomly over time. On the contrary, with SPS, fewer messages get lost, but this occurs through a several losses in a row, leading ultimately to worse AoI values.

We observe that for DS, the average AoI between all pairs increases only slightly as the distance between vehicles grows, with all values clustering around the overall average. In contrast, for SPS the situation is different: the average AoI

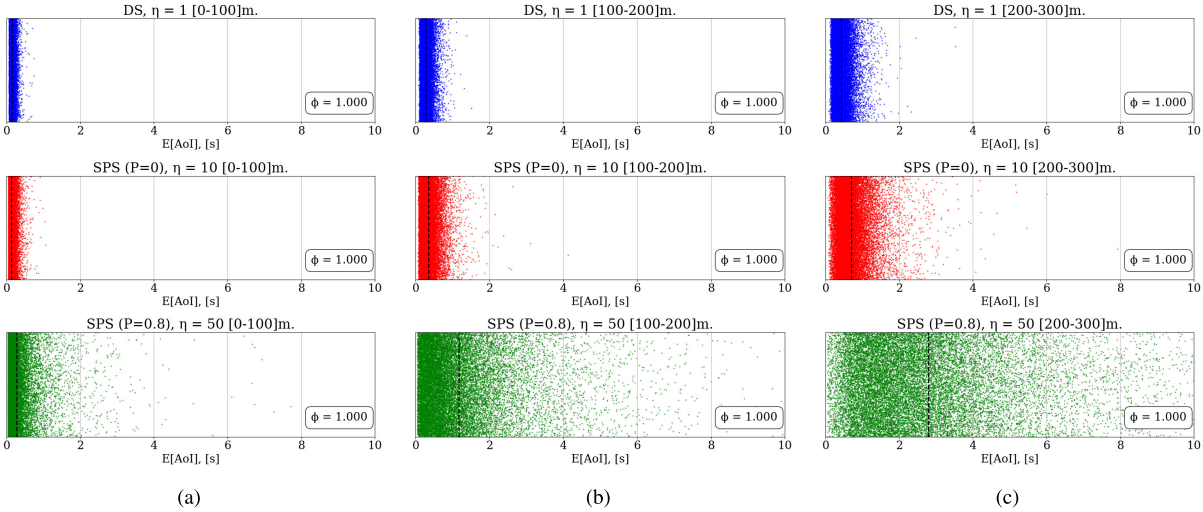

FIGURE 11. Scatter plots of mean AoI values for each vehicle pair for three persistence settings. Three different distance ranges are considered: (a) [0;100] m; (b) [100;200] m; (c) [200;300] m;.

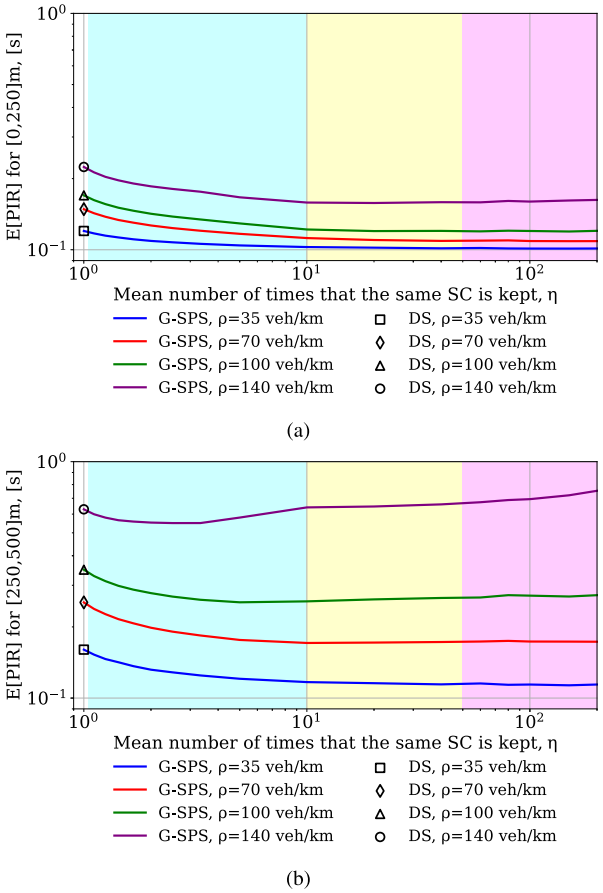

FIGURE 12. E[PIR] as a function of η for different persistence classes and for different vehicle densities with 1 SC: (a) [0,250]m; (b) [250,500]m.

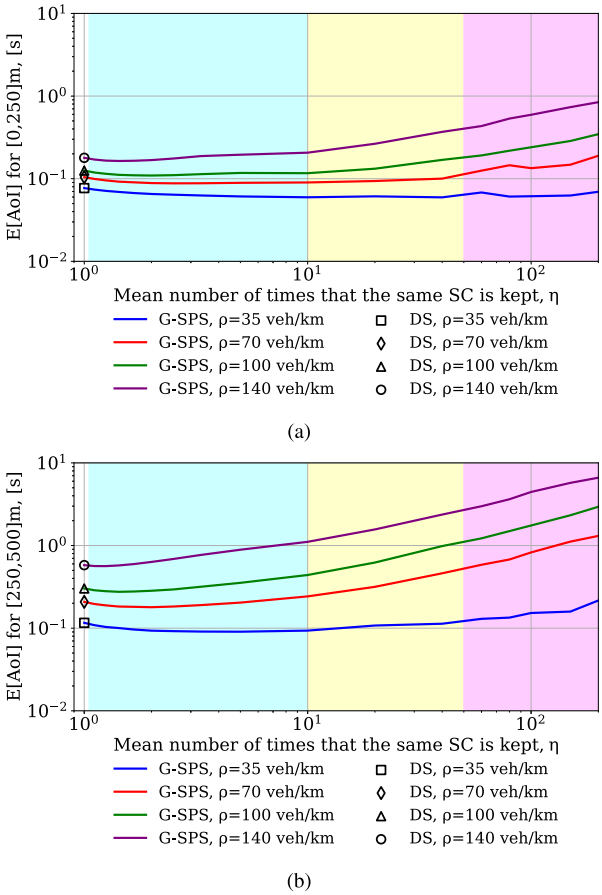

FIGURE 13. E[AoI] as a function of η for different persistence classes and for different vehicle densities with 1 SC: (a) [0,250]m; (b) [250,500]m.

increases rapidly, along with the spread of values around the average.

The analysis of the values of $\mathrm{E}[A_{i\to j}]$ marks another point in favor of the adoption of DS. It appears that, for all distance ranges, not only is the overall average AoI better, but values of AoI experienced by different vehicle pairs are less spread out, in a sense offering more reliable and "fairer" performance.

Analogous to the analysis in Figure 6, we investigate the behavior of PIR and AoI under varying vehicle densities, considering a single SC with 50 RBs. Figure 12 and Figure 13 depict the performance of PIR and AoI, respectively, as a function of η for four different vehicle densities, ranging from 140 veh/km down to 35 veh/km. The analysis considers two distance intervals: [0,250] m and [250,500] m.

It is evident that PIR performance degrades as vehicle density increases. Moreover, as the inter-vehicle distance grows, the gap between PIR values for different densities becomes increasingly pronounced. Notably, at short distances, this gap remains minimal for densities ranging from 35 to 100 veh/km but increases sharply at 140 veh/km. This can be attributed to the fact that a density of 140 veh/km closely approximates the worst-case traffic scenario in terms of vehicular congestion. For short distances, PIR exhibits consistent behavior across all densities once moderate persistence is reached, reaffirming the optimality of high persistence in minimizing PIR at close range. However, as the distance between vehicles increases, we observe that densities between 35 and 100 veh/km continue to demonstrate similar trends, while the highest density (140 veh/km) exhibits non-monotonic behavior, as previously observed in Figure 9a. Overall, it is apparent that in most cases, persistence has a limited impact on PIR across different traffic densities. Additionally, PIR performance remains generally sufficient to meet application requirements, reinforcing the robustness of the system under varying traffic conditions.

The most interesting aspect in terms of performance analysis across various vehicle densities stems from mean AoI curves presented in Figure 13. In all considered parameter settings for vehicle density, persistence and distance range, mean AoI exhibits a minimum that occurs in the weak persistence region, further confirming the need for standard expansion. Even at low vehicle densities, collisions can occur, and the duration of these collisions becomes a decisive factor affecting AoI performance. When analyzing the persistence classes corresponding to DS and SPS, we observe that for short distances (up to 250 m), SPS slightly outperforms DS. As the distance increases, we see that for any vehicle density, DS yields better mean AoI with respect to SPS, in spite of message flow generation for each vehicle being periodic, hence fit to SPS logic.

In addition to analyzing PRR, we extend our investigation to assess the impact of different channel configurations – specifically, 1, 2, and 5 SCs on PIR and AoI. A thorough understanding of the underlying simulation setup is essential for an accurate interpretation of the results. To ensure a consistent comparison, we maintain a fixed vehicle density (140 veh/km) across all configurations. However, increasing the number of SC effectively provides more available radio resources within a single RRI. To preserve an equivalent network load across different configurations, we proportionally adjust both the RRI duration and the packet generation interval according to the number of SCs. This approach ensures that the total number of transmitted messages remains

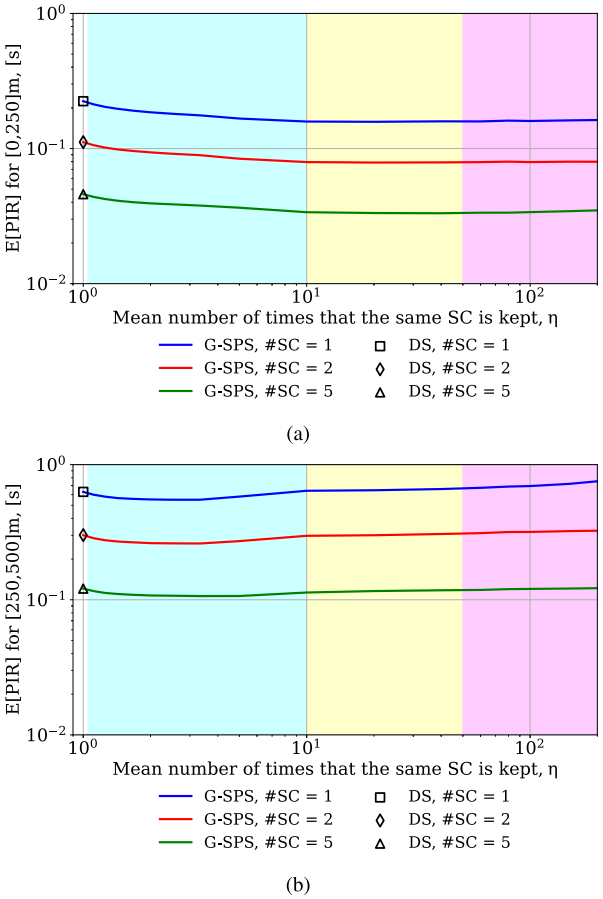

FIGURE 14. E[PIR] as a function of η for different persistence classes and for different number of SCs with density of 140 veh/km: (a) [0,250]m; (b) [250,500]m.

constant across all simulations, where the total simulation time is normalized to 1000 RRIs. The specific RRI values for each configuration are as follows: 1 SC: RRI = 100 ms, 2 SC: RRI = 50 ms, 5 SC: RRI = 20 ms. This adjustment is crucial when analyzing the simulation results, as it ensures a fair evaluation of the system's behavior under different channel allocations.

Figures 14 and 15 present the performance analysis of PIR and AoI across different channel configurations as a function of persistence. The results indicate that PIR behavior remains remarkably consistent across all channel configurations and distances, showing minimal variation with persistence. The observed differences in absolute values are primarily attributed to the varying RRI values across simulations. Notably, when PIR is normalized to RRI, the quantitative metrics become identical across all channel configurations, further reinforcing the stability of PIR under different allocation schemes.

A similar trend is observed for AoI. Regardless of the specific channel configuration, AoI exhibits a consistent behavioral pattern, characterized by a distinct minimum within the weak persistence region. Additionally, when averaged over the distance intervals [0,250] m and [250,500]

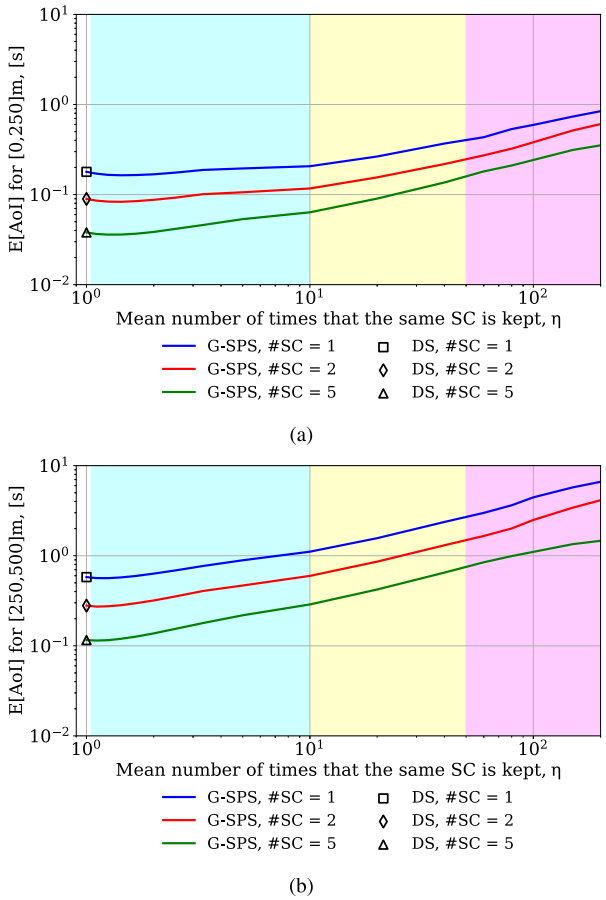

FIGURE 15. E[AoI] as a function of η for different persistence classes and for different number of SCs with density of 140 veh/km: (a) [0,250]m; (b) [250,500]m.

m, the DS scheme demonstrates higher AoI values compared to SPS, further confirming the trends identified in previous analyses.

These findings highlight the robustness of the proposed framework, demonstrating that the choice of channel configuration has a negligible impact on PIR and AoI dynamics under the given simulation conditions. Nevertheless, it is crucial to acknowledge that the channel configuration directly affects the available TB size for data transmission. In particular, a single SC with 50 RB allows for a TB size of 1473 Byte, whereas dividing the channel into two SCs with 25 RB per SC reduces the TB size to 528 Byte. When further subdividing into five SCs, each with 10 RB, the available TB size decreases to 217 Byte. These variations must be taken into account when analyzing performance results, as they directly influence the maximum amount of data that can be successfully transmitted within a single transmission opportunity, potentially impacting higher-layer protocol efficiency and overall system throughput.

C. WRAP-UP DISCUSSION

The results of this section lead to the following key remarks:

1) **Simplification of the standard SPS**: As shown in Figures 5 and 9, the performance of G-SPS ($\overline{RC} = 1$) is equivalent to that of the standard SPS. This suggests that the RC parameter can be removed from the standard, simplifying the resource allocation algorithm.
2) **Extension of persistence performance range**: G-SPS enables a seamless range of persistence levels, spanning from DS to strong persistence, effectively eliminating the gaps present in the current standard. These gaps have led many researchers to identify the lowest possible persistence probability value $P = 0$ as the optimal choice for standard SPS. However, this value represents only a local minimum, constrained by the limited flexibility of the standard SPS. The broader range provided by G-SPS allows for more precise system tuning, enabling the selection of the most suitable persistence class to meet specific application requirements.
3) **DS outperforms SPS in terms of AoI for periodic update traffic in highway scenarios with hidden nodes**: In the specific yet critical case of periodic update message flows, SPS offers minimal advantage and may even result in worse performance (as measured by AoI, the most relevant metric for this type of traffic) compared to DS. While persistence may occasionally provide some benefit, it is typically marginal. This is illustrated by the dispersion plots: in DS, message losses between relationships $i \rightarrow j$ are more frequent but random, whereas in SPS, losses are correlated and tend to occur in consecutive bursts, which further disrupts communication.
4) **Achieving minimal mean AoI values**: The minimum AoI values can be achieved for any vehicle density and channel configuration. Previously, these values could not be attained due to the absence of weak persistence in the standard. These results were first obtained for a realistic highway scenario with hidden nodes and the possibility of SCs reuse. This highlights the importance of using G-SPS in 5G NR-V2X sidelink. Since AoI reflects the freshness of information received by vehicles from their neighbors, minimizing it is critically important for road safety.

VIII. CONCLUSION

This paper provides an in-depth and impactful analysis of medium access control mechanisms in 5G New Radio (NR)-Vehicle-to-Everything (V2X) sidelink communications, specifically focusing on periodic update message flows in highway scenarios with hidden nodes. Through large-scale simulations conducted in the ns-3 environment, we investigate key aspects of persistence management and resource allocation, offering valuable insights to improve the design and optimization of 5G NR-V2X systems.

We introduce a novel framework for defining and classifying persistence in resource allocation algorithms for

5G NR-V2X communications. Our proposed Geometric Semi-Persistent Scheduling (G-SPS) model simplifies and enhances persistence management by offering a more flexible definition, capable of accommodating a broader range of configurations compared to the traditional Semi-Persistent Scheduling (SPS). Unlike SPS, which requires multiple parameters, G-SPS can be implemented with just one parameter, improving both efficiency and ease of application. By removing the Reselection Counter (RC) parameter, G-SPS streamlines the SPS mechanism without sacrificing effectiveness. We demonstrate that G-SPS consistently delivers optimal Age of Information (AoI) performance, outperforming SPS in terms of both mean values and quantiles. Furthermore, G-SPS improves the tail properties of persistence by reducing the likelihood of re-iterated collisions, enhancing robustness in highly congested scenarios. Ultimately, G-SPS simplifies persistence implementation in 5G NR-V2X communications while maintaining high performance. These results highlight the potential of G-SPS as a viable alternative in certain traffic scenarios, laying the groundwork for future research aimed at refining persistence models and optimizing communication protocols for vehicular networks.

Our analysis also uncovers the trade-offs involved in persistence management. Strong persistence improves Packet Reception Ratio (PRR) and communication stability but leads to increased AoI due to slower resource switching. On the other hand, weak persistence minimizes AoI while maintaining acceptable PRR values by effectively balancing collision rates and durations. This nuanced understanding emphasizes the need for context-specific persistence strategies tailored to the demands of Intelligent Transportation Systems (ITS) applications.

A critical finding of our study is that Dynamic Scheduling (DS) outperforms SPS in scenarios involving periodic update message flows and hidden nodes. While SPS exhibits bursty loss patterns that disrupt consecutive updates, DS introduces randomized loss dynamics, significantly improving AoI and enhancing communication robustness. This insight positions DS as a more resilient and effective solution for minimizing AoI in periodic update scenarios, surpassing the standard SPS mechanism.

In conclusion, this study provides a robust analytical and experimental foundation for advancing the design of 5G NR-V2X sidelink communications. By addressing challenges such as hidden nodes, vehicular density, and persistence management, we offer actionable recommendations for optimizing network performance. These findings are expected to drive future developments in resource allocation strategies, ultimately enhancing the reliability and efficiency of intelligent transport systems.

REFERENCES

[1] S. Nikooroo, J. Estrada-Jimenez, A. Machalek, J. Härri, T. Engel, and I. Turcanu, "Mitigating collisions in sidelink NR V2X: A study on cooperative resource allocation," in *Proc. 22nd Medit. Commun. Comput. Netw. Conf. (MedComNet)*, Jun. 2024, pp. 1–4.

[2] S. Bhadauria, K. Plaku, Y. Deshpande, and W. Kellerer, "Evaluation of NR-sidelink for cooperative industrial AGVs," in *Proc. IEEE 21st Consum. Commun. Netw. Conf. (CCNC)*, Jan. 2024, pp. 777–783.

[3] M. H. C. Garcia, A. Molina-Galan, M. Boban, J. Gozalvez, B. Coll-Perales, T. Sahin, and A. Kousaridas, "A tutorial on 5G NR V2X communications," *IEEE Commun. Surveys Tuts.*, vol. 23, no. 3, pp. 1972–2026, 3rd Quart., 2021.

[4] *Overall Description of Radio Access Network (RAN) Aspects for Vehicle-to-Everything (V2X) Based on LTE and NR (3GPP TR 37.985 Version 18.0.0)*, document TR 37.985, 3GPP, Dec. 2023.

[5] *NR; Radio Resource Control (RRC) Protocol Specification (Release 18)*, document TS 38.331, 3GPP, Jun. 2025.

[6] *NR; Medium Access Control (MAC) Protocol Specification (Release 18)*, document TS 38.321, 3GPP, Jun. 2025.

[7] A. Rolich, I. Turcanu, A. Vinel, and A. Baiocchi, "Impact of persistence on the age of information in 5G NR-V2X sidelink communications," in *Proc. 21st Medit. Commun. Comput. Netw. Conf. (MedComNet)*, Jun. 2023, pp. 15–24.

[8] A. Rolich, I. Turcanu, A. Vinel, and A. Baiocchi, "Understanding the impact of persistence and propagation on the age of information of broadcast traffic in 5G NR-V2X sidelink communications," *Comput. Netw.*, vol. 248, Jun. 2024, Art. no. 110503.

[9] *Digital Cellular Telecommunications System (Phase 2+) (GSM); Universal Mobile Telecommunications System(UMTS); LTE; 5G; Release 16 Description; Summary of Rel-16 Work Items (3GPP TR 21.916 Version 16.2.0 Release 16)*, document TR 121 916, ETSI, Jul. 2022.

[10] *5G; NR; Physical Layer Procedures for Data (3GPP TS 38.214 Version 19.0.0 Release 19)*, document TS 38.214, 3GPP, Jun. 2025.

[11] *Study on Evaluation Methodology of New Vehicle-to-Everything (V2X) Use Cases for LTE and NR; (Release 15)*, document TR 37.885, 3GPP, Jun. 2019.

[12] A. Molina-Galan, J. Gozalvez, and B. Coll-Perales, "A selective re-evaluation mechanism for 5G NR V2X mode 2 communications," *IEEE Trans. Veh. Technol.*, early access, Aug. 11, 2025, doi: 10.1109/TVT.2025.3597549.

[13] M. Elsharief, S. Rahman Sabuj, N. Jeong, and H.-S. Jo, "Advancing NR-V2X: Evaluating mode 2 performance through analytical modeling and simulations," *IEEE Access*, vol. 13, pp. 141636–141650, 2025.

[14] J. Guerra, M. Luís, and P. Rito, "Performance evaluation of 5G new radio V2X sidelink for coexisting traffic," *IEEE Access*, vol. 13, pp. 131400–131410, 2025.

[15] M. Montaño and R. Cajo, "Full-duplex resource reselection scheme for mixed periodic and aperiodic traffic in 5G NR-V2X sidelink," in *Proc. IEEE Veh. Netw. Conf. (VNC)*, Jun. 2025, pp. 305–312.

[16] A. Bazzi, V. Todisco, A. Molinaro, A. O. Berthet, R. A. Stirling-Gallacher, and C. Campolo, "Exploiting repetitions and interference cancellation for the 6G-V2X sidelink autonomous mode," *IEEE Trans. Veh. Technol.*, early access, Jul. 23, 2025, doi: 10.1109/TVT.2025.3592028.

[17] C. Campolo, V. Todisco, A. Molinaro, A. Berthet, S. Bartoletti, and A. Bazzi, "Improving resource allocation for beyond 5G V2X sidelink connectivity," in *Proc. 55th Asilomar Conf. Signals, Syst., Comput.*, Oct. 2021, pp. 55–60.

[18] C. Campolo, A. Bazzi, V. Todisco, S. Bartoletti, N. Decarli, A. Molinaro, A. O. Berthet, and R. A. Stirling-Gallacher, "Enhancing the 5G-V2X sidelink autonomous mode through full-duplex capabilities," in *Proc. IEEE 95th Veh. Technol. Conf. (VTC-Spring)*, Jun. 2022, pp. 1–6.

[19] V. Todisco, S. Bartoletti, C. Campolo, A. Molinaro, A. O. Berthet, and A. Bazzi, "Performance analysis of sidelink 5G-V2X mode 2 through an open-source simulator," *IEEE Access*, vol. 9, pp. 145648–145661, 2021.

[20] L. Lusvarghi and M. L. Merani, "Machine learning for disseminating cooperative awareness messages in cellular V2V communications," *IEEE Trans. Veh. Technol.*, vol. 71, no. 7, pp. 7890–7903, Jul. 2022.

[21] L. Lusvarghi, A. Molina-Galan, B. Coll-Perales, J. Gozalvez, and M. L. Merani, "A comparative analysis of the semi-persistent and dynamic scheduling schemes in NR-V2X mode 2," *Veh. Commun.*, vol. 42, Aug. 2023, Art. no. 100628.

[22] L. Lusvarghi, M. L. Merani, F. Pasquinucci, and M. Andreani, "Dynamic scheduling in NR-V2X mode 2: Probability of successful packet delivery and packet inter-reception," *IEEE Trans. Veh. Technol.*, early access, Jun. 24, 2025, doi: 10.1109/TVT.2025.3583092.

[23] A. Chourasia, B. R. Tamma, and A. Antony Franklin, "Traffic-aware sensing-based semi-persistent scheduling for high efficacy of C-V2X networks," in *Proc. IEEE 94th Veh. Technol. Conf. (VTC-Fall)*, Sep. 2021, pp. 1–5.

[24] J. Wu, Y. Guo, and S. Zhou, "A reliable self-adaptive scheduling control protocol for cellular V2X mode 4," *IEEE Access*, vol. 10, pp. 63991–64003, 2022.

[25] J. Yan and J. Härri, "MCS analysis for 5G-NR V2X sidelink broadcast communication," in *Proc. IEEE Intell. Vehicles Symp. (IV)*, Jun. 2022, pp. 1347–1352.

[26] A. Rehman, R. Valentini, E. Cinque, P. Di Marco, and F. Santucci, "On the impact of multiple access interference in LTE-V2X and NR-V2X sidelink communications," *Sensors*, vol. 23, no. 10, p. 4901, May 2023.

[27] Z. Ali, S. Lagén, L. Giupponi, and R. Rouil, "3GPP NR V2X mode 2: Overview, models and system-level evaluation," *IEEE Access*, vol. 9, pp. 89554–89579, 2021.

[28] F. Romeo, C. Campolo, A. Molinaro, and A. O. Berthet, "Asynchronous traffic on the sidelink of 5G V2X," in *Proc. IEEE Int. Conf. Commun. Workshops (ICC Workshops)*, Jun. 2020, pp. 1–6.

[29] G. G. Md. Nawaz Ali, S. A. Sharief, M. N. Sadat, and M. S. Miah, "Performance analysis of 5G new radio V2X communication," in *Proc. IEEE Wireless Microw. Technol. Conf. (WAMICON)*, Apr. 2023, pp. 1–4.

[30] E. E. González, Y. Estrada, D. Garcia-Roger, and J. F. Monserrat, "Performance evaluation and optimal management of mode 2 V2X communications in 5G networks," *IEEE Access*, vol. 11, pp. 128810–128825, 2023.

[31] V. Todisco, C. Campolo, A. Molinaro, A. O. Berthet, R. A. Stirling-Gallacher, and A. Bazzi, "Full duplex based collision detection to enhance the V2X sidelink autonomous mode," *Comput. Netw.*, vol. 254, Dec. 2024, Art. no. 110763.

[32] V. Todisco, Z. Wu, and A. Bazzi, "Improving NR-V2X autonomous mode through resource re-evaluation," in *Proc. IEEE Veh. Netw. Conf. (VNC)*, May 2024, pp. 125–131.

[33] J. Yin and S.-H. Hwang, "Reuse distance-aided resource selection mechanisms for NR-V2X sidelink communication," *Sensors*, vol. 24, no. 1, p. 253, Dec. 2023.

[34] D. Wang, P. B. Mohite, Q. Zhou, A. Qiu, and H. D. Schotten, "Evaluating the impact of numerology and retransmission on 5G NR V2X communication at a system-level simulation," in *Proc. IEEE Conf. Standards Commun. Netw. (CSCN)*, Nov. 2023, pp. 59–65.

[35] L. Zhao, J. Hu, R. Zhao, and Y. Shi, "The enhanced sidelink resource reservation mechanism of NR-V2X," in *Proc. IEEE 96th Veh. Technol. Conf. (VTC-Fall)*, Sep. 2022, pp. 1–5.

[36] C. Brady, L. Cao, and S. Roy, "Modeling of NR C-V2X mode 2 throughput," in *Proc. IEEE Int. Workshop Tech. Committee Commun. Quality Rel. (CQR)*, Sep. 2022, pp. 19–24.

[37] R. D. Yates, Y. Sun, D. R. Brown, S. K. Kaul, E. Modiano, and Ş. Ulukuş, "Age of information: An introduction and survey," *IEEE J. Sel. Areas Commun.*, vol. 39, no. 5, pp. 1183–1210, May 2021.

[38] W.-D. Shen and H.-Y. Wei, "Age of information performance analysis in power-efficient sidelink communications," *IEEE Internet Things J.*, early access, Aug. 4, 2025, doi: 10.1109/JIOT.2025.3595400.

[39] E. Markova, V. E. Manaeva, E. Zhbankova, D. Moltchanov, P. Balabanov, Y. Koucheryavy, and Y. Gaidamaka, "Performance-utilization trade-offs for state update services in 5G NR systems," *IEEE Access*, vol. 12, pp. 129789–129803, 2024.

[40] M. Bezmenov, A. Munari, Z. Utkovski, and S. Stanczak, "Age of information for V2X: Irregular repetition slotted ALOHA and semi-persistent scheduling," in *Proc. IEEE Int. Conf. Commun.*, Jun. 2024, pp. 1023–1028.

[41] M. Bezmenov, Z. Utkovski, and S. Stanczak, "The impact of blind retransmissions on the age of information in NR-V2X," in *Proc. IEEE 100th Veh. Technol. Conf. (VTC-Fall)*, Oct. 2024, pp. 1–6.

[42] A. Bazzi, C. Campolo, A. Molinaro, A. O. Berthet, B. M. Masini, and A. Zanella, "On wireless blind spots in the C-V2X sidelink," *IEEE Trans. Veh. Technol.*, vol. 69, no. 8, pp. 9239–9243, Aug. 2020.

[43] A. Bazzi, G. Cecchini, A. Zanella, and B. M. Masini, "Study of the impact of PHY and MAC parameters in 3GPP C-V2V mode 4," *IEEE Access*, vol. 6, pp. 71685–71698, 2018.

[44] Y. Yoon and H. Kim, "A stochastic reservation scheme for aperiodic traffic in NR V2X communication," in *Proc. IEEE Wireless Commun. Netw. Conf. (WCNC)*, Mar. 2021, pp. 1–6.

[45] L. Cao, S. Roy, and H. Yin, "Resource allocation in 5G platoon communication: Modeling, analysis and optimization," *IEEE Trans. Veh. Technol.*, vol. 72, no. 4, pp. 5035–5048, Apr. 2023.

[46] L. Cao, H. Yin, R. Wei, and L. Zhang, "Optimize semi-persistent scheduling in NR-V2X: An age-of-information perspective," in *Proc. IEEE Wireless Commun. Netw. Conf. (WCNC)*, Apr. 2022, pp. 2053–2058.

[47] T. E. T. Djaidja, B. Brik, S. M. Senouci, and Y. Ghamri-Doudane, "Adaptive resource reservation to survive against adversarial resource selection jamming attacks in 5G NR-V2X distributed mode 2," in *Proc. IEEE Int. Conf. Commun.*, May 2022, pp. 3406–3411.

[48] A. Rolich, I. Turcanu, and A. Baiocchi, "AoI-aware and persistence-driven congestion control in 5G NR–V2X sidelink communications," in *Proc. 22nd Medit. Commun. Comput. Netw. Conf. (MedComNet)*, Jun. 2024, pp. 1–4.

[49] A. Rolich, M. Yildiz, I. Turcanu, A. Vinel, and A. Baiocchi, "On the trade-off between AoI performance and resource reuse efficiency in 5G NR V2X sidelink," in *Proc. IEEE Veh. Netw. Conf. (VNC)*, Jun. 2025, pp. 1–8.

[50] L. Lusvarghi and M. L. Merani, "MoReV2X—A new radio vehicular communication module for ns-3," in *Proc. IEEE 94th Veh. Technol. Conf. (VTC-Fall)*, Sep. 2021, pp. 1–7.

[51] L. Lusvarghi. (2024). *MoReV2X*. [Online]. Available: https://github.com/LLusvarghi/MoReV2X

[52] L. Lusvarghi, B. Coll-Perales, J. Gozalvez, and M. L. Merani, "Link level analysis of NR V2X sidelink communications," *IEEE Internet Things J.*, vol. 11, no. 17, pp. 28385–28397, Sep. 2024.

[53] *Enhancement of 3GPP Support for V2X Scenarios; Stage 1 (Release 18)*, document TS 22.186, 3GPP, Mar. 2024.

ALEXEY ROLICH (Member, IEEE) received the bachelor's and master's degrees from the National Research University Higher School of Economics, Moscow, Russia, in 2013 and 2015, respectively, and the Ph.D. degree from the University of Rome La Sapienza, in 2025. He is currently a Researcher with the Department of Information Engineering, Electronics and Telecommunications, University of Rome La Sapienza. He is the author of more than 20 publications in international journals and conference proceedings. His research interests include vehicular networks, medium access control protocols, cellular radio networks, simulations, and performance evaluation. He was a recipient of the Mario Gerla Best Paper Award at the 21st Mediterranean Communication and Computer Networking Conference (MedComNet 2023).

MERT YILDIZ (Graduate Student Member, IEEE) received the bachelor's degree in industrial engineering from Yaşar University, İzmir, Türkiye, and the master's degree in data science from Sapienza University of Rome, Italy, where he is currently pursuing the Ph.D. degree with the Department of Information Engineering, Electronics, and Telecommunications. Throughout his academic career, he has worked with several companies, leveraging his expertise to address practical challenges in optimizing complex systems. His research interests include system optimization, workload generation, queueing theory, and performance evaluation of large-scale distributed systems.

ION TURCANU (Senior Member, IEEE) received the M.Sc. degree in computer science and the Ph.D. degree in information and communication technologies from the University of Rome Sapienza, Italy, in 2014 and 2018, respectively. He is currently the Head of the Networking and Communications Group, Luxembourg Institute of Science and Technology. His research interests include next-generation mobile networks, cooperative networked systems, network digital twins, connected and automated mobility, and time-sensitive networking. He has served on the technical and executive committees of several conferences, including the TPC Co-Chair for the 2024 MedComNet, the Poster/Demo Co-Chair for the 2024 IEEE VNC, and the Publicity Co-Chair for the 2023 IEEE VNC. Since 2025, he has been on the editorial board of *IEEE Vehicular Technology Magazine* and *Vehicular Communications* (Elsevier).

ALEXEY VINEL (Senior Member, IEEE) received the Ph.D. degree from Tampere University of Technology, Finland, in 2013. He is currently a Professor with Karlsruhe Institute of Technology (KIT), Germany. Before he joined KIT, in October 2022, he was a Professor at the University of Passau, Germany. Since 2015, he has been a Professor at Halmstad University, Sweden (now part-time). He has led several research projects, including the Knowledge Foundation Synergy Project SafeSmart, from 2019 to 2024. His research interests include vehicular communications and cooperative autonomous driving. He was a recipient of the Alexander von Humboldt Foundation Fellowship, in 2008.

ANDREA BAIOCCHI (Member, IEEE) received the Laurea degree in electronics engineering and the Ph.D. degree in information and communications engineering from the University of Rome Sapienza, in 1987 and 1992, respectively. Since January 2005, he has been a Full Professor at the Department of Information Engineering, Electronics and Telecommunications, University of Rome Sapienza. He has published more than 170 papers in international journals and conference proceedings. He is the author of the book *Network Traffic Engineering–Stochastic Models and Applications* (Wiley, 2020). His main scientific contributions are in telecommunications network traffic engineering, queuing theory, resource sharing, and congestion control. His current research interests include massive multiple access and vehicular networking. His research activities have also been carried out in the framework of many national (CNR, MIUR, and POR) and international (European Union and ESA) projects, also taking coordination and responsibility roles. He has participated in the technical program committees of 80 international conferences. He also served on the editorial board of the telecommunications technical journal published by Telecom Italia (currently TIM) for ten years. He is currently Associate Editor of *Vehicular Communications* journal (Elsevier).